Morphometric Analysis of Retinal Pigment Epithelial Cells From C57BL/6J Mice During Aging

Yong-Kyu Kim,[1,2] Hanyi Yu,[3] Vivian R. Summers,[1] Kevin J. Donaldson,[1] Salma Ferdous,[1] Debresha Shelton,[1] Nan Zhang,[1,4] Micah A. Chrenek,[1] Yi Jiang,[5] Hans E. Grossniklaus,[1] Jeffrey H. Boatright,[1,6] Jun Kong,[3,5,7] and John M. Nickerson[1]

[1]Department of Ophthalmology, Emory University School of Medicine, Atlanta, Georgia, United States
[2]Department of Ophthalmology, Hallym University College of Medicine, Kangdong Sacred Heart Hospital, Seoul, South Korea
[3]Department of Computer Science, Emory University, Atlanta, Georgia, United States
[4]Department of Ophthalmology, Second Xiangya Hospital of Central South University, Changsha, Hunan, China
[5]Department of Mathematics and Statistics, Georgia State University, Atlanta, Georgia, United States
[6]Atlanta VA Center for Visual and Neurocognitive Rehabilitation, Decatur, Georgia, United States
[7]Department of Computer Science, Georgia State University, Atlanta, Georgia, United States

Correspondence: John M. Nickerson, Department of Ophthalmology, Emory University, B5602, 1365B Clifton Road NE, Atlanta, GA 30322, USA;
litjn@emory.edu.

Received: August 1, 2020
Accepted: February 1, 2021
Published: February 22, 2021

Citation: Kim Y-K, Yu H, Summers VR, et al. Morphometric analysis of retinal pigment epithelial cells from C57BL/6J mice during aging. *Invest Ophthalmol Vis Sci.* 2021;62(2):32. https://doi.org/10.1167/iovs.62.2.32

Purpose. To quantitatively evaluate the changes in orientation and morphometric features of mouse retinal pigment epithelial (RPE) cells in different regions of the eye during aging.

Methods. We segmented individual RPE cells from whole RPE flatmount images of C57BL/6J mice (postnatal days 30 to 720) using a machine-learning method and evaluated changes in morphometric features, including our newly developed metric combining alignment and shape of RPE cells during aging.

Results. Mainly, the anterior part of the RPE sheet grows during aging, while the posterior part remains constant. Changes in size and shape of the peripheral RPE cells are prominent with aging as cells become larger, elongated, and concave. Conversely, the central RPE cells maintain relatively constant size and numbers with aging. Cell count in the central area and the overall cell count (approximately 50,000) were relatively constant over different age groups. RPE cells also present a specific orientation concordance that matches the shape of the specific region of the eyeball. Those cells near the optic disc or equator have a circumferential orientation to cover the round shape of the eyeball, whereas those cells in the periphery have a radial orientation and corresponding radial elongation, the extent of which increases with aging and matches with axial elongation of the eyeball.

Conclusions. These results suggest that the fluid RPE morphology reflects various growth rates of underlying eyeball, and RPE cells could be classified into four regional classes (near the optic disc, central, equatorial, and peripheral) according to their morphometric features.

Keywords: aging, cell size, machine learning, mice, retinal pigment epithelium

The retinal pigment epithelium (RPE) is a monolayer of regularly packed polygonal cells located between the choroid and the neural retina. The main functions of the RPE are to support the visual function of photoreceptors, reinforce the choriocapillaris through vascular endothelial growth factor secretion, and act as a barrier.[1,2] Although RPE cells are known to have regular shapes and spatial organization, they can also deform locally to fill in gaps as the basic characteristics of epithelia.[3] In previous studies, we found that the quantitative analysis of RPE sheet morphology, particularly the RPE cell area and its aspect ratio, allowed discrimination of mouse age and strain.[4] In a human cadaver eye study, RPE cells differed in area and shape by region and age.[5–9] These findings indicate that morphometric features of RPE cells can be indicators of the cell pathophysiologic status.

The RPE is known to be a quiescent cell with limited proliferation ability.[10,11] However, the ocular tissue underneath the RPE continues to grow during development and aging. In a study on growth and development of the mouse RPE, the RPE surface area increased about 10-fold from embryonic day 15 to adulthood, whereas the number of RPE cells increased only about fourfold during the same period. This suggests that much of the increase in tissue size results from the increase in individual cell size rather than in the cell number.[12] Studies on human RPE also suggest that there is a net decrease in the overall density of RPE cells without major RPE loss during aging.[5–9,13]

These prior studies suggest that the RPE cell size tends to increase with age, and this change in cell size may differ by eyeball region; however, in previous studies, cell area information was estimated by counting the number of cells in representative small regions across a much larger area of the full sheet.[11,13,14] With such methods, it was not possible to evaluate the variation in cell size or various morphometric features, including cell shape and orientation. In prior studies, we selected and cropped 45 to 60 representative regions of equal size from the whole merged flatmount image.[4,15,16] Despite these efforts, the RPE sheet area used for analysis represented only a small proportion of the total area. These evaluations did not include individual cell spatial or orientation information. Thus, in this work, we evaluated the morphometric features of each RPE cell in a whole RPE flatmount image using a machine-learning-based, single-cell segmentation method. In particular, we evaluated whether the RPE cell patterns indicate the varying degree of eyeball growth in the different regions during aging by quantitative RPE cell morphometric analyses. For this purpose, we have proposed a novel morphometric metric that combines cell spatial alignment and shape information.

Methods

Mouse RPE Flatmount Preparation

In this study, we analyzed selected flatmount images in our accumulated reference database, which we previously described.[4,16] We selected two of the best-prepared C57BL/6J mouse RPE flatmount images per each age group (postnatal day 30 [P30], P45, P60, P180, and P330) and four RPE flatmount images of P720 C57BL/6J mice from our database (images are available at the Cell Image Library, http://cellimagelibrary.org/groups/52245). We chose images without major gross defects or tissue deformation and images that were taken under even illumination. Mouse information and details regarding the RPE flatmount preparation technique are provided in the previous literature.[4,16] The animals were treated according to the ARVO Statement for the Use of Animals in Ophthalmic and Vision Research, and the study was approved by the Emory University School of Medicine Institutional Animal Care and Use Committee.

RPE Flatmount Image Segmentation

For morphometric analysis of individual RPE cells in each flatmount image, we segmented RPE cells in flatmount images (Fig. 1A). We extracted the green-channel image that captured cell borders stained with ZO-1 (Fig. 1B). Using a machine-learning-based ImageJ (National Institutes of Health, Bethesda, MD, USA) plugin, Trainable Weka Segmentation,[17] the image was binarized (Fig. 1C). Following a sequence of steps including despeckling, skeletonization, and abnormally segmented cell removal in a semi-automatic way, cells with artifacts were removed from further analysis, such as those in tissue foldings or cells at the cut edge (Figs. 1G–1J). These processing steps result in the skeletonized images with thin cell borders (1 pixel in thickness). The percentage of the analyzed image area varied according to the overall staining quality. Such analyzed image region percentages were generally low near the optic disc and in the periphery (Fig. 2K). The overall percentage of the analyzed area was 53.7% ± 8.8% (Fig. 2L).

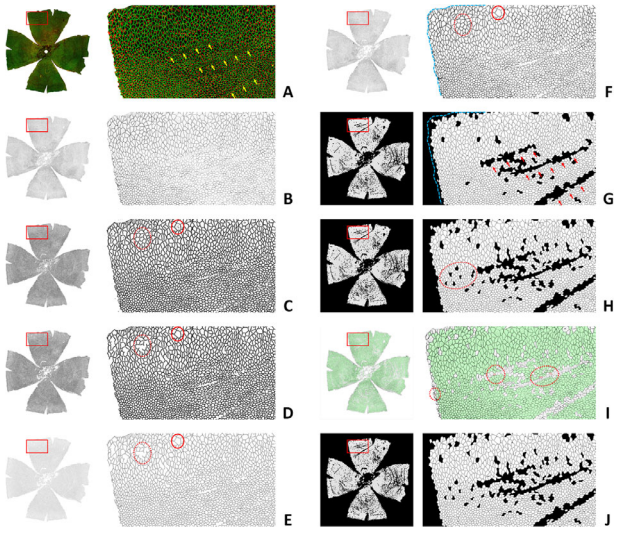

Figure 1. Flatmount RPE cell segmentation. Serially processed RPE flatmount images are presented. Magnified images are the corresponding area of the *red rectangle* on whole flatmount images. (**A**) Mouse RPE flatmount was stained for ZO-1 (*green*) and nucleus (propidium iodide, *red*). Artifacts (folds) made during the flatmount preparation are indicated with *yellow arrows*. (**B**) Green-channel image. A signal from green fluorescence (ZO-1 staining) was extracted. (**C**) Binarized image. Using the machine-learning-based ImageJ plugin Trainable Weka Segmentation, the image was binarized. (**D**) Despeckling. Particles less than 100 pixels in size were removed from the image; however, this process also removed cell boundaries with minor discontinuity (*red dotted circles* in **C** and **D**) as well as small particles inside the cell areas (*red circles* in **C** and **D**). (**E**) Skeletonization. The image was skeletonized with thin cell borders. After the noise signal inside the cell was removed (*red circle*), some cells had missing boundaries (*red dotted circle*). (**F**) Image adjustment. Comparing the pixel intensity between the original image (green-channel image, **B**) and binary skeletonized image (**E**), the missing boundaries were recovered (*red dotted circle*), and speckles were suppressed (*red circle*). (**G**) Removing cells with unconnected lines or touching the cut edges of the flatmount. Cells without complete boundaries inside the cell area particularly near the artifact were removed (*red arrows*). Cells on the cut edges of the flatmount (*blue dotted line* in **F** and **G**) were also removed, as these cells are likely to be damaged during flatmount preparation. (**H**) Cell removal according to the area and morphology criteria. Cells less than 20 pixels or greater than 2000 pixels were removed. Those with solidity (cell area/convex area) less than 3 SDs from the mean of each zone were also removed. These concave areas result from the undersegmentation of multiple cells (*red dotted circle*). (**I**) Manual cell removal. Using our developed MATLAB-based graphical application, we overlaid the original green-channel image with the segmented image. All cell candidates were labeled by a green mask initially. We then clicked on the erroneously segmented cells, which are represented by a red mask (in *red dotted circles*). Cells in red masks were removed from further analysis. We carefully examined the cut edges of the flatmount and regions with artifacts such as tissue folding, and we eliminated any damaged cells from those areas. (**J**) The final analysis image set was prepared. These steps generally eliminated 30% to 50% of the RPE cells from the area of the whole flatmount.

Morphometric Analysis

Using the skeletonized image with thin cell borders (1 pixel in thickness), we performed several morphometric

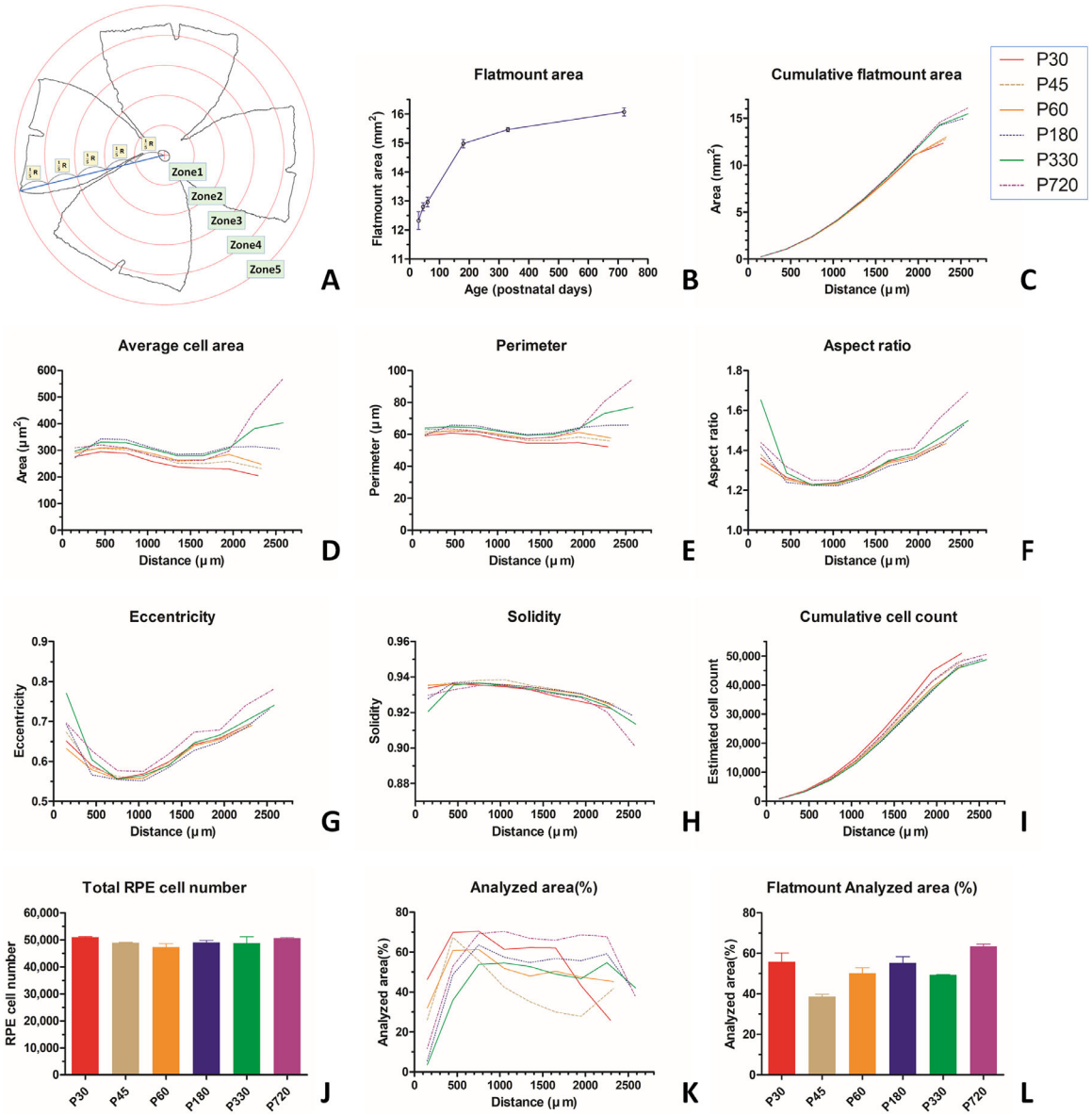

Figure 2. Morphological analysis of RPE cells in different age groups. Two flatmount images from each of five age groups (P30, P45, P60, P180, P330) and four flatmount images from P720 were analyzed. (**A**) Zone segmentation. The radius (R) was defined as the distance from the center of the optic disc to the farthest point of the flatmount. Each image was evenly divided into five zones by such distance. Each corresponding concentric zone was designated by zone 1 (center) to zone 5 (periphery). (**B**) The flatmount area monotonously increased until P180, and after that the rate of increase decreased. (**C**) The increase rate of the cumulative flatmount area was constant until 1200 μm; however, it was higher in the old group after a distance of 1200 μm. (**D**) Average cell area. Young mice showed decreased cell size from center to periphery. As the mice got older, cell size increased in the peripheral area. Overall, the average cell size was larger in the old group, particularly in zone 1 (young, 296.9 ± 8.8 μm^2; old, 324.3 ± 16.3 μm^2; $P = 0.003$), zone 4 (young, 253.2 ± 18.8 μm^2; old, 304.4 ± 13.8 μm^2; $P < 0.001$), and zone 5 (young, 234.6 ± 20.8 μm^2; old 436.2 ± 94.2 μm^2; $P < 0.001$, *t*-test). (**E**) The change in cell perimeter showed a similar pattern to the average cell area. (**F**) The aspect ratio (major axis length/minor axis length) was high near the optic disc and in the periphery. The aspect ratio was significantly greater in the old group in zones 3, 4, and 5: zone 3, 1.26 ± 0.01 for young mice versus 1.30 ± 0.03 for old mice ($P = 0.016$); zone 4, 1.35 ± 0.01 for young mice versus 1.39 ± 0.04 for old mice ($P = 0.011$); zone 5, 1.43 ± 0.02 for young mice versus 1.56 ± 0.10 for old mice ($P = 0.005$). (**G**) Eccentricity showed a similar pattern to the aspect ratio. The eccentricity was large near the optic disc and in the periphery. The eccentricity of old mice was greater than that of the young mice. (**H**) Solidity (area/convex area) showed a decreasing pattern from the center to the periphery, in particular, zone 5 cells showed a stronger decrease as the mice got older: 0.924 ± 0.001 for young mice versus 0.917 ± 0.006 for old mice ($P = 0.007$). (**I**) There was no significant difference in the cumulative estimated cell count increase rate according to the distance from the optic disc center between 0 to 1200 μm range; however, the cell count increased rapidly in the young group between 1200 μm and 2400 μm. (**J**) The estimated total cell number was constant over the different age groups with an average of 49,403 ± 1711 cells per eye. (**K**, **L**) Percentage of the analyzed area over the total flatmount area. The mean overall percentage of the analyzed area was 53.7%. The percentage of the analyzed area dropped near the optic disc and in the far periphery.

Investigative Ophthalmology & Visual Science

analyses. We calculated the morphologic characteristics of each cell including cell area, length of the major and minor axes, eccentricity (the ratio of the distance between the foci of the ellipse best fit to the cell to its major axis length), solidity (cell area/convex area), perimeter, aspect ratio (major axis length/minor axis length), and circularity ($[4 \times \text{area} \times \pi]/\text{perimeter}^2$). Cells are expected to present various morphological changes to adapt to the local environment. These changes can include cell elongation or reduction in the shape convexity to compensate for the loss of the neighboring cells. With the cell area and perimeter measurements, we compared the overall cell size in different age groups and regions. We evaluated the degree of cellular elongation by the eccentricity and the aspect ratio, and we also evaluated morphological irregularity by the solidity and circularity.

As the cell density in mouse species has been reported to present a well-defined variation in radial but not circumferential directions,[14] and we found no significant cell size variation according to the circumferential direction (Supplementary Fig. S1), we only analyzed the data according to the distance from the center of the optic disc. The morphometric analysis was performed in two ways. First, we divided five zones by the distance between the center of the optic disc and the center of each cell (Fig. 2A) and calculated the average value of each morphometric feature in each zone. Second, we repeated the same analysis but by the actual distance from the center of the optic disc. Each zone has a 300-µm interval in the radial direction, and the average value of each morphometric feature in each zone was calculated. We calculated the percentage of abnormal cells by size in each zone. We defined the outlier cells as those with size greater than three scaled median absolute deviations (MADs), where MAD is defined as $\text{median}(|A_i - \text{median}(A)|)$ for $i = 1, 2, \ldots, N$. The scaled MAD is defined as $c \times \text{MAD}$, where $c = 1.4826$.[18,19] The cell count in each zone was calculated by dividing the flatmount area in each zone by the average cell size. These cell counts were summed to estimate the total RPE cell numbers.

In this study, we combined the cell orientation and cell shape to measure cell radial orientation. First, we calculated angle θ between the major axis of the cell and the line connecting the center of the optic disc and the center of the cell (Fig. 3A). Note that the expression $\cos\theta \times$ (major axis length–minor axis length)/major axis length increases as angle θ decreases, thus suggesting the cell radial alignment in reference to the optic disc center. When the aspect ratio (major axis length/minor axis length) increases, the expression also increases, suggesting cells in a more elongated shape (Fig. 3B).

With cell morphometric features including the cell area, convex area, length of the major and the minor axes, perimeter, circularity, solidity, eccentricity, aspect ratio, and radial cell orientation, principal component analysis (PCA) was performed on different age groups and zones. As one more step further from the PCA results, we performed linear discriminant analysis (LDA) to evaluate whether cell morphometric features can be used to predict the age or cell zone. Cells were divided into two groups according to the region (zones 1–4 vs. zone 5) and age groups (P30–P60 vs. P180–P720), respectively. The classification accuracy was evaluated with the K-fold cross-validation method with fold number 10.[20] All analysis was performed with MATLAB (version R2019b; The MathWorks, Inc., Natick, MA, USA). All MATLAB scripts used for the analysis are provided at GitHub (https://github.com/ykkim7/Matlab-codes-for-FM-image-analysis).

Results

Rate of Increase in Flatmount Area Differs by Region and the Anterior Part of the Eye Grows Mainly With Age

The flatmount area increased as mice got older. The rate of increase was high in an early postnatal phase (P30–P180, linear regression gave 0.017 mm^2/day), whereas it slowed in the late postnatal phase (P180–720, linear regression gave 0.002 mm^2/day) (Fig. 2B). We divided mice into two age groups, young (P30–P60) and old (P180–P720) based on the largest change in the flatmount area and morphometric features between age P60 and P180. When we analyzed the cumulative flatmount area from the optic disc center at 300-µm intervals, the increase rate of the cumulative flatmount area remained constant until a distance of 1200 µm (young, linear regression showed an increase rate of 4289.8 μm^2/µm; old, 4383.9 μm^2/µm). Linear mixed model analysis showed that there was no significant interaction between age groups and the distance from the center of the optic disc in this range. However, the cumulative flatmount area increase rate between distances of 1200 µm and 2400 µm was higher in the old group (young, 7353.6 μm^2/µm; old, 8959.7 μm^2/µm). Linear mixed model analysis showed a significant interaction between age groups and the distance from the center of the optic disc in this range, suggesting a significant difference in the flatmount area increase rate between the two groups (beta coefficient $[\beta] = 1606.0$, $P < 0.001$) (Fig. 2C).

Peripheral Cells Grow More Than the Central Cells and Abnormally Large Cells Appear in the Central Area During Aging

For young mice, the average cell size showed a decreasing trend toward the periphery; however, cells in zone 5 showed a dramatic size increase for older mice. Overall, the average cell size was larger in the old group, particularly in zones 1, 4, and 5 (Fig. 2D). The percentage of the outliers was larger in the old group in zones 1, 2, and 3; however, the percentage of the outliers was larger in the young group in zone 4 (Supplementary Fig. S2). The perimeter showed a similar pattern for average cell size (Fig. 2E).

Cells Become Elongated and Concave, Particularly in the Periphery With Age

The aspect ratio (major axis length/minor axis length) was high near the optic disc and in the periphery. The aspect ratio was significantly greater in the old group in zones 3, 4, and 5 (Fig. 2F). The eccentricity (the ratio of the distance between the foci of the ellipse best fit to the cell to its major axis length) showed a similar pattern to the aspect ratio (Fig. 2G). The solidity (cell area/convex area) showed a decreasing pattern from the center to the periphery, in particular, zone 5 cells showed a stronger decrease as the mice got older (Fig. 2H).

Investigative Ophthalmology & Visual Science

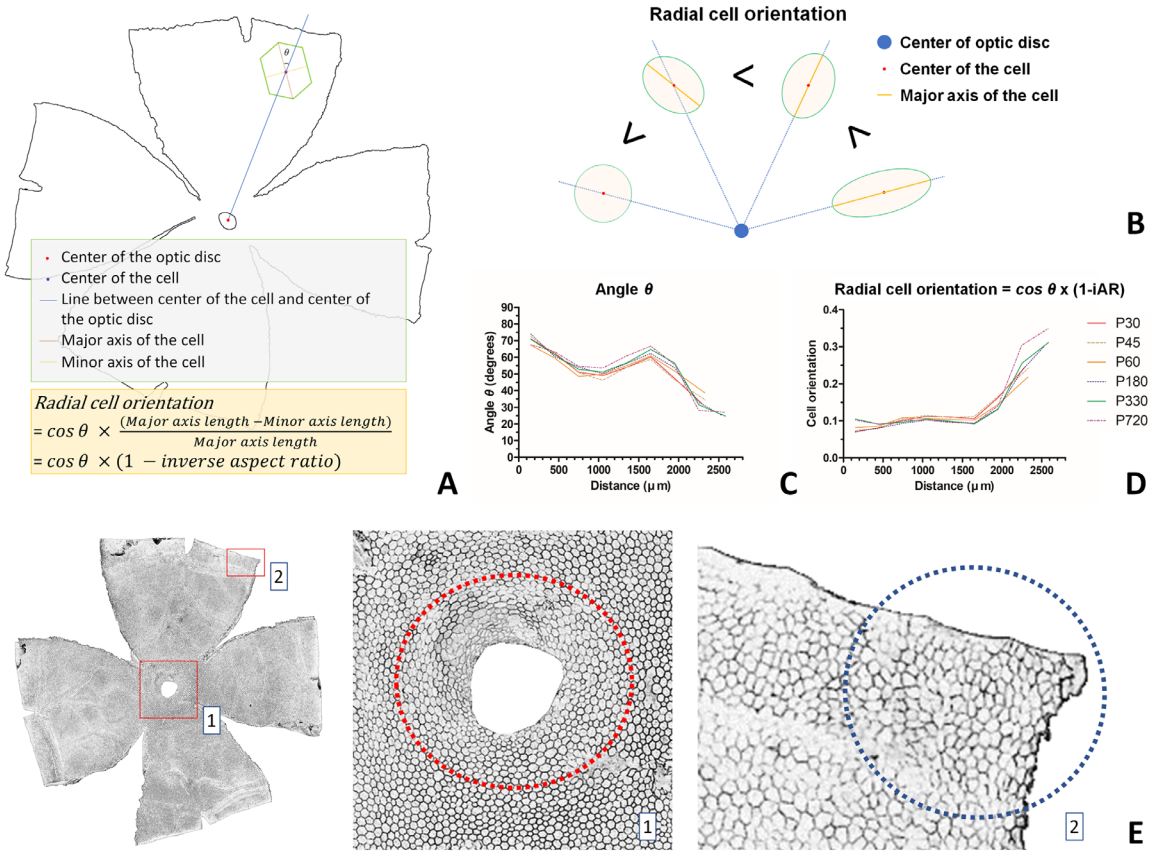

Figure 3. A measure of the degree of radial cell orientation. (**A**) The degree of cells oriented radially outward was calculated by (1) the angle between the major axis of the cell and the line connecting the center of the optic disc and the center of the cell, and (2) the cell aspect ratio. The equation $\cos\theta \times \frac{(major\ axis\ length - minor\ axis\ length)}{major\ axis\ length}$ increases when angle θ decreases, and the inverse aspect ratio, *iAR* = minor axis length/major axis length, decreases. (**B**) Illustration of changes in angle θ and aspect ratio of the cell and corresponding changes in the radial cell orientation. When the major and the minor axes of the cell length are the same, the aspect ratio becomes 1, and the radial cell orientation becomes 0 (far left). When the cell is elongated, the radial cell orientation increases (second from left). When the cell is oriented toward the center, the radial cell orientation further increases (third from left). When the cell is oriented toward the center and the cell is more elongated toward the major axis direction, the radial cell orientation further increases (far right). (**C**) Changes in angle θ are demonstrated as a function of the distance from the optic disc center. Angle θ showed a decreasing trend from the center to the periphery, with a second hump appearing between 1600 µm and 1700 µm. Angle θ of the old group was greater than that of the young group from 600 µm to 2100 µm; however, it was greater in the young group between 2100 µm and 2400 µm (young, 35.1° ± 3.4°; old, 30.2° ± 2.7°; $P = 0.012$). (**D**) Changes in the radial cell orientation according to distance from the optic disc center. Changes in the radial cell orientation showed a relatively constant level until 1800 µm; however, it rapidly increased in the periphery. The old mice group showed a higher value of radial cell orientation at the periphery compared to the young group. (**E**) Flatmount images from P30 mouse. The area in *red rectangles* on whole flatmount images are magnified. Cells near the optic disc (*red dotted circle*) are elongated and encircle the optic disc margin. Thus, the major axis and the line between the optic disc center and the center of the cell form large angles. On the other hand, cells in the periphery (*blue dotted circle*) were radially outwardly oriented, making angle θ small and the radial cell orientation large.

Cell Count in the Central Area and the Overall Cell Count Were Relatively Constant Over Different Age Groups

There was no significant difference in the cumulative estimated cell count increase rate between 0 and 1200 µm (young, linear regression gave an increase rate of 14.8 cells/µm; old, 14.2 cells/µm). Linear mixed model analysis showed that there were no significant interactions between age groups and the distance from the center of the optic disc in this range. On the contrary, the estimated cell count increase rate was higher in the young group at distances between 1200 µm and 2400 µm (young, 29.8 cells/µm; old, 28.4 cells/µm), and the linear mixed model analysis showed a marginal significance in interactions between age groups and the distance from the center of the optic disc in this range (β =1.35; $P = 0.068$) (Fig. 2I). There was no significant difference in estimated total cell count between young and old mice (young, 49,000.4 ± 1873.2; old, 49,704.3 ± 1640.2; $P = 0.468$) (Fig. 2J).

Cells Orient Radially Outwardly in the Periphery, Whereas Cells Orient Circumferentially Near the Optic Disc and in the Mid-Periphery

The angle between the major axis of the cell and a line connecting the center of the optic disc and the center of the cell (angle θ) reached the largest value for cells near the optic disc and showed a decreasing trend toward the periph-

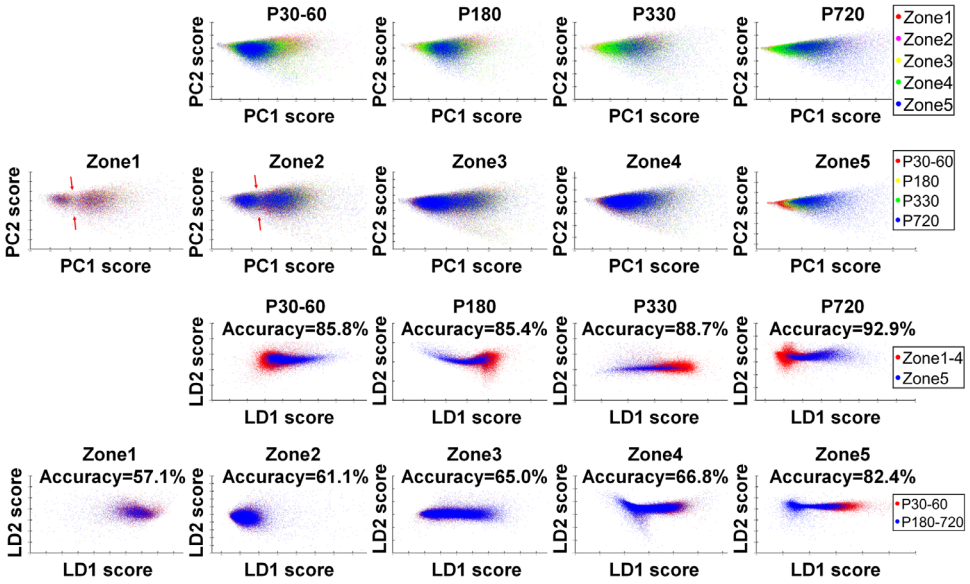

Figure 4. Results of PCA and LDA. With cell morphometric features, PCA was performed on different age groups and different zones. LDA was also performed to evaluate whether cell morphometric features can be used to predict the age or cell zone. (*Top row*) PCA with different age groups. In young mice groups (P30–60), cells from different zones were clumped in the same cluster. As mice got older (P180–720), the zone 5 cells were separated from the other cell cluster. (*Second row*) PCA in different zones. In zones 1 through 4, cells from different age groups were clustered together. Two clusters of cells in zones 1 and 2 along the PC1 (*red arrows* dividing the clusters) were observed. As zone number increased, a stronger pattern of a serial separation of cells from young to old mice appeared. (*Third row*) LDA was performed to discriminate far peripheral cells (zone 5) from other cells. Zone 5 cells can be discriminated from others using morphometric features in all age groups with an accuracy greater than 85%. (*Bottom row*) LDA was performed to discriminate cells of old mice (P180–P720) from those of young mice (P30–P60). The discrimination accuracy was between 57.1% and 66.8% in zones 1 through 4. The discrimination accuracy for zone 5 was the highest (82.4%).

ery, with a second hump appearing between 1500 µm and 1800 µm. To find a more detailed location of the second hump, we calculated the average angle θ every 50 µm, and the highest angle value of the second hump appeared between 1600 µm and 1650 µm radially in P30, P45, P60, and P720 mice and between 1650 µm and 1700 µm radially in P180 and P330 mice. Angle θ of the old group was greater than that of the young group in the range of 600 µm to 2100 µm; however, it was greater in the young group between 2100 µm and 2400 µm (Fig. 3C).

Peripheral Cells Become More Radially Oriented and Elongated With Age

The radial cell orientation, characterized by the expression cos θ × (1 – inverse aspect ratio), showed a relatively constant level until 1800 µm radially; however, it was substantially increased, approaching the periphery beyond that. The average value of the radial cell orientation was greater in the young group compared to that of the old group between 600 µm and 2100 µm, whereas it was greater in the old group between 2100 µm and 2400 µm (young, 0.24 ± 0.02; old, 0.27 ± 0.03; P = 0.026). The average value of the radial cell orientation was even larger in P720 mice compared to P180 to P330 mice in the periphery: from 2100 µm to 2400 µm, 0.25 ± 0.01 for P180 to P330 versus 0.30 ± 0.02 for P720 (P = 0.003); from 2400 µm to the edge, 0.31 ± 0.01 for P180 to P330 versus 0.35 ± 0.01 for P720 (P = 0.002) (Fig. 3D).

Principal Component Analysis and Linear Discriminant Analysis

PCA results were plotted with the first two principal components (PCs). In all analyses, the first PC (PC1) explained more than 99.7% of the total variance and both PC1 and the second PC (PC2) explained more than 99.99% of the total variance. The major components of the PC1 were cell area (component coefficient 0.66 to 0.68) and convex area (component coefficient 0.73 to 0.75). The major components of the PC2 were cell area (component coefficient 0.68 to 0.72), convex area (component coefficient –0.63 to –0.57), and perimeter (component coefficient –0.34 to –0.25). PCA results showed that cells from different zones were clumped in the same cluster in the young mice group (P30–P60), whereas zone 5 cells were more separated from the other cluster for older mice (Fig. 4, first row). For zones 1 through 4, cells from different age groups were clustered together; however, we observed two clusters of cells in zones 1 and 2 along the PC1 (red arrows dividing the clusters). In zone 5, cells were sequentially separated from younger to older mice (Fig. 4, second row). The result of the LDA was plotted with the first two linear discriminant components. The zone 5 cells could be discriminated from others in all age groups with an accuracy greater than 85% (Fig. 4, third row). The cells from old mice (P180–P720) could be discriminated from those from the young age group (P30–P60) with an accuracy between 57.1% and 66.8% in zones 1 through 4 and an accuracy of 82.4% in zone 5 (Fig. 4, bottom row).

Investigative Ophthalmology & Visual Science

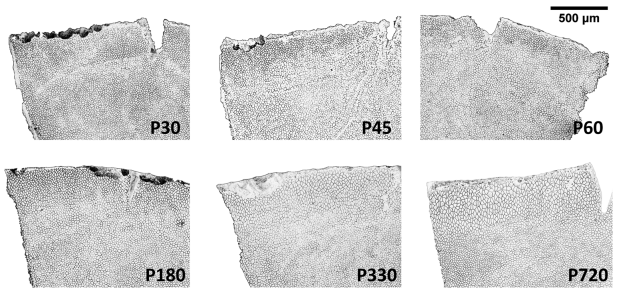

Figure 5. Peripheral images of the RPE flatmount in different age groups. In these same scaled images, we can see the gradual changes in the far peripheral cells that become dysmorphic, enlarged, and elongated.

Discussion

In this study, we performed a morphometric analysis of RPE cells using the whole RPE flatmount images. By using the whole image rather than using its cropped parts, we could analyze spatial and orientation information, as well as the morphological features of each cell. Furthermore, our newly developed metric, radial cell orientation, which combined alignment and shape of each cell, gave us a clue regarding how RPE cells change during aging, especially in the periphery. Several studies on ocular growth in C57BL/6J mice have reported an increase in axial length with age[21–26]; however, it is unclear whether the eyeball grows at the same rate in all areas. Although we did not directly measure the eyeball size, we compared the cumulative flatmount area according to the distance from the optic disc center and revealed that the flatmount area from the optic disc center to a distance of 1200 µm was almost the same in all age groups. This suggests that the posterior pole of the eyeball maintains its original curvature and shape, whereas the anterior part of the eye grows mainly with age. However, further detailed study on changes in eyeball shape and size with aging is necessary.

The mouse RPE cell showed a significant morphological change with age. Overall, cell size increases, and cells become elongated and concave with age; however, these age-dependent changes in RPE cells mainly occurred in the periphery (Fig. 5). On the other hand, the central cells maintained a relatively constant average cell size and numbers. There was no significant change in estimated total cell count during aging, with approximately 50,000 consistently from P30 to P720 mice. This number is similar to that from the previous report of approximately 54,000.[14]

In this study, we developed a new metric combining alignment and shape to evaluate dynamic changes of the RPE cell during aging. The radial cell orientation showed a relatively constant level until 1800 µm radially. However, it was substantially increased approaching the periphery beyond that. Interestingly, even in young mice, although the peripheral cells were smaller than the central cells, they were more elongated in shape and presented a stronger radial orientation. The degree of radial cell orientation even increased from P330 to P720. According to the information available at The Jackson Laboratory (Bar Harbor, ME, USA), P180, P330, and P720 mice are considered mature adults, middle-aged, and old, respectively, in human age equivalents.[27] Thus, the change in the degree of radial cell orientation could result from the peripheral RPE maturation and the physical stress related to eyeball growth after birth.

Jeffery et al.[28–30] revealed in a series of studies that the peripheral mouse RPE cells have proliferative properties. A recent single-cell RNA sequencing study also showed that human peripheral RPE cells showed increased expression of TFPI2, promoting RPE proliferation in vitro.[31,32] Combining these previous reports with our current result suggests that the newly emerged surface anterior to the equator as aging is mainly filled by the proliferating peripheral cells. Previous researchers have also suggested that proliferating peripheral cells might be a source to replenish RPE cells[8,28]; however, our results do not suggest a large migration of cells. First, cells in the periphery and those in the center presented a huge difference in shape. Furthermore, cells associated with the second peak of angle θ, which can be thought of as a locational marker, maintained their physical locations as the mice became older and eyeballs got larger. This suggests that the primary mode of RPE sheet expansion is a rearrangement in place with limited replenishment in the far periphery rather than extensive peripheral replenishment and a shift of the new peripheral cells migrating into the central parts of the sheet.

Our findings are in line with the basic functions of the RPE—that is, protecting the retina by forming a barrier and supporting the visual function of the photoreceptors. In our study, the size of the posterior pole and the number of RPE cells in that area remained relatively constant over all ages. Although mice do not have a macula, the central region of the mouse retina shares some features with the human macula.[33] The RPE number is known to be closely correlated with the number of rod and cone cells.[34] Thus, it can be expected that a significant change in eyeball shape and RPE topography in the central region might affect vision. It is known that more binucleated cells are located centrally than in the periphery.[11,14] Chen et al.[11] suggested that an increase in cell size and multinucleation may be a strategy for RPE cells to repair damage during aging. In this study, we did not count the nucleus numbers; however, the PCA result showed that there were two clusters of cells in zones 1 and 2 along the PC1 that is mostly associated with cell size. As binucleate cells are known to be larger than mononucleate cells,[14] the two cell clusters might represent mono- and binucleate cells, respectively.

In summary, the central RPE cells remained largely unchanged in size or number and can be expected to cope with cellular damage and maintain a focus more on visual function. In contrast, cells at the periphery were found to be mainly focused on covering the extended surface area of the eyeball. Changes in the basic orientation of RPE cells and changes that occur throughout aging in different regions of the eyeball are summarized in Figure 6. We suggest a model of four regional classes of RPE cells: (1) Cells in the posterior polar area near the optic disc are circumferentially oriented and stretched. (2) Small and regularly shaped RPE cells have two different sizes (possibly smaller mononucleate and larger binucleate cells) in the central to the mid-peripheral area. Although there is no significant difference in the average size, the cell size varies more, and abnormally large cells appear in older mice. (3) Equatorial RPE cells are stretched and oriented circumferentially to cover the broad area of the equatorial band. (4) Far peripheral cells are large and dysmorphic due to stretching on radial coordinates. The cells become more irregular in shape with aging.

There are several limitations to the current investigation. The flatmounts we used for the evaluation were not completely flat; however, we took precautions to avoid wrin-

Investigative Ophthalmology & Visual Science

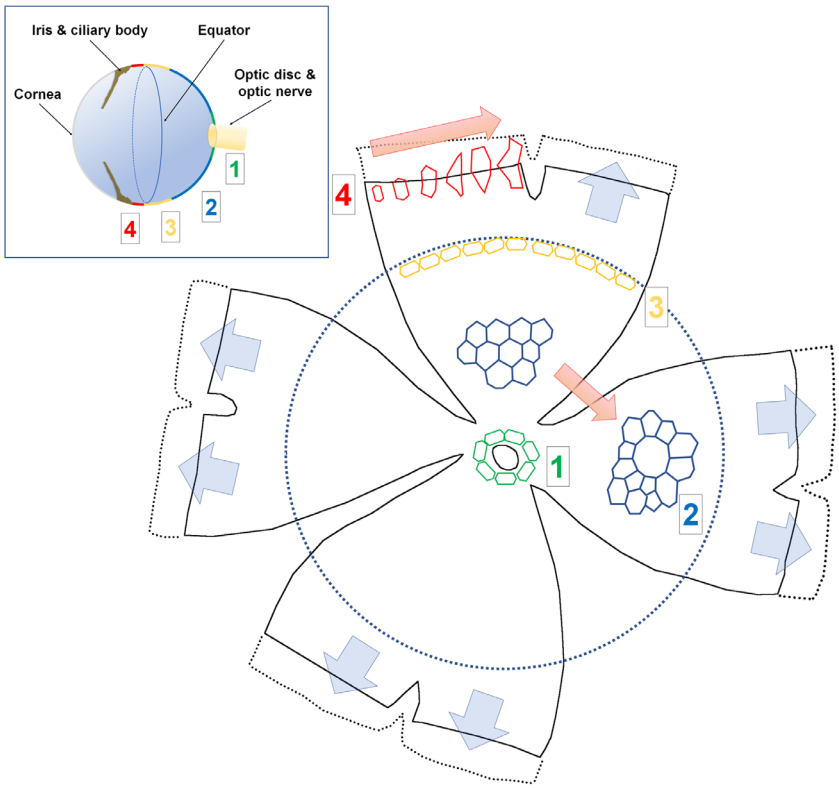

Figure 6. Summary illustration of eyeball growth and RPE cell changes with aging. Each number in the schematic of the eyeball in the upper left corner and the flatmount image represents the same region. *Blue arrows* in the flatmount image represent axial elongation of the eyeball during aging. *Red arrows* in the flatmount image represent changes in RPE morphology during aging. *Blue dotted* circles in the schematic of the eyeball and the flatmount image represent the equator. (1) Cells in the posterior polar area near the optic disc are elongated in shape and encircle the optic disc. (2) Cells in the central to mid-peripheral area do not change significantly in numbers and average size; however, the cell size varies more, and abnormally large cells appear as mice get older. (3) Cells near the equator are elongated and encircle the equatorial band, to cover the largest area of the RPE surface. (4) Cells in the periphery are oriented outward and show a dramatic change in cell size and shape during aging. Cells become bigger and dysmorphic and seem to cover most of the stretched area during eyeball growth.

kling by not over-fixing the tissue, thus making it more pliant and easier to flatten. The possibility of tissue tilting was reduced by flattening the tissue with a much larger cover glass than the flatmount tissue. In addition, only the best images were carefully selected and used for analysis in this study. We excluded images with major tissue folds, defects, or uneven illumination due to surface irregularity from further analysis. The ZO-1 signal located in the apex of the cell was used for cell segmentation, and the possibility of *z*-plane error was reduced by the maximum intensity projection method. Those warped cells near the tissue fold were excluded from the analysis, and sample unevenness was averaged out because of two factors: (1) we used a large number of cells for every single eye analysis, and (2) on average, for every cell that is compressed, an equal number of cells are stretched; that is, compression and stretching balance out with going up, over, and down for any given protrusion.

Although we tried our best to accurately segment individual RPE cells, there was still a small portion of mis-segmented cells. Deep learning algorithms such as the convolutional neural network can be a good alternative solution for enhanced segmentation; however, deep learning methods require a large scale of well-annotated training datasets. Unfortunately, it is not easy to create such a training dataset with whole RPE flatmount images. The semiautomatic methods developed in this study can be used to help facilitate the dataset creation necessary for training deep learning algorithms in the future. We segmented RPE cells by the signal from the apical tight junctions (ZO-1) only; however, the actual RPE cell is three dimensional.[35] Finally, we did not evaluate the number of nuclei. It was difficult to distinguish the RPE nucleus signal from cells in the underlying choroid, and it was also difficult to determine whether an RPE cell nucleus was located in one cell or its neighbor.

In conclusion, there were clear topographic differences in RPE cell morphology, and these all change with age. The central RPE cells have a relatively constant level of cell size and numbers throughout the ages; however, peripheral cells had a large degree of radial extension responding to the axial elongation of the eyeball. Those cells near the optic disc or the equator were arranged in a direction to encircle the underlying round shape of the eye. Further studies of age-related changes in eyeball dimensions and corresponding morphological and cytoskeletal changes in RPE are necessary to understand damage responses and normal growth responses in the RPE.

Acknowledgments

Supported by Grants from the National Institutes of Health (R01EY028450, R01EY021592, P30EY006360, U01CA242936,

Investigative Ophthalmology & Visual Science

F31EY028855, R01EY028859, T32EY07092, T32GM008490); by the Abraham J. and Phyllis Katz Foundation; by grants from the U.S. Department of Veterans Affairs and Atlanta Veterans Administration Center for Excellence in Vision and Neurocognitive Rehabilitation (RR&D I01RX002806, I21RX001924; VA RR&D C9246C); and an unrestricted grant to the Department of Ophthalmology at Emory University from Research to Prevent Blindness, Inc.

Disclosure: **Y.-K. Kim**, None; **H. Yu**, None; **V.R. Summers**, None; **K.J. Donaldson**, None; **S. Ferdous**, None; **D. Shelton**, None; **N. Zhang**, None; **M.A. Chrenek**, None; **Y. Jiang**, None; **H.E. Grossniklaus**, None; **J.H. Boatright**, None; **J. Kong**, None; **J.M. Nickerson**, None

References

1. Strauss O. The retinal pigment epithelium in visual function. *Physiol Rev*. 2005;85(3):845–881.
2. Kanow MA, Giarmarco MM, Jankowski CS, et al. Biochemical adaptations of the retina and retinal pigment epithelium support a metabolic ecosystem in the vertebrate eye. *eLife*. 2017;6:e28899.
3. Guillot C, Lecuit T. Mechanics of epithelial tissue homeostasis and morphogenesis. *Science*. 2013;340(6137):1185–1189.
4. Jiang Y, Qi X, Chrenek MA, et al. Functional principal component analysis reveals discriminating categories of retinal pigment epithelial morphology in mice. *Invest Ophthalmol Vis Sci*. 2013;54(12):7274–7283.
5. Bhatia SK, Rashid A, Chrenek MA, et al. Analysis of RPE morphometry in human eyes. *Mol Vis*. 2016;22:898–916.
6. Gao H, Hollyfield JG. Aging of the human retina. Differential loss of neurons and retinal pigment epithelial cells. *Invest Ophthalmol Vis Sci*. 1992;33:1–17.
7. Harman AM, Fleming PA, Hoskins RV, Moore SR. Development and aging of cell topography in the human retinal pigment epithelium. *Invest Ophthalmol Vis Sci*. 1997;38(10):2016–2026.
8. Del Priore LV, Kuo YH, Tezel TH. Age-related changes in human RPE cell density and apoptosis proportion in situ. *Invest Ophthalmol Vis Sci*. 2002;43(10):3312–3318.
9. Ach T, Huisingh C, McGwin G, Jr, et al. Quantitative autofluorescence and cell density maps of the human retinal pigment epithelium. *Invest Ophthalmol Vis Sci*. 2014;55(8):4832–4841.
10. Stern J, Temple S. Retinal pigment epithelial cell proliferation. *Exp Biol Med (Maywood)*. 2015;240(8):1079–1086.
11. Chen M, Rajapakse D, Fraczek M, Luo C, Forrester JV, Xu H. Retinal pigment epithelial cell multinucleation in the aging eye – a mechanism to repair damage and maintain homoeostasis. *Aging Cell*. 2016;15(3):436–445.
12. Bodenstein L, Sidman RL. Growth and development of the mouse retinal pigment epithelium. II. Cell patterning in experimental chimaeras and mosaics. *Dev Biol*. 1987;121(1):205–219.
13. Ts'o MO, Friedman E. The retinal pigment epithelium. 3. Growth and development. *Arch Ophthalmol*. 1968;80(2):214–216.
14. Bodenstein L, Sidman RL. Growth and development of the mouse retinal pigment epithelium. I. Cell and tissue morphometrics and topography of mitotic activity. *Dev Biol*. 1987;121(1):192–204.
15. Chrenek MA, Dalal N, Gardner C, et al. Analysis of the RPE sheet in the rd10 retinal degeneration model. *Adv Exp Med Biol*. 2012;723:641–647.
16. Boatright JH, Dalal N, Chrenek MA, et al. Methodologies for analysis of patterning in the mouse RPE sheet. *Mol Vis*. 2015;21:40–60.
17. Arganda-Carreras I, Kaynig V, Rueden C, et al. Trainable Weka Segmentation: a machine learning tool for microscopy pixel classification. *Bioinformatics*. 2017;33(15):2424–2426.
18. Huber PJ. *Robust Statistics*. New York: John Wiley & Sons; 2004.
19. Leys C, Ley C, Klein O, Bernard P, Licata L. Detecting outliers: do not use standard deviation around the mean, use absolute deviation around the median. *J Exp Soc Psychol*. 2013;49(4):764–766.
20. Stone M. Cross-validatory choice and assessment of statistical predictions. *J R Stat Soc Series B Stat Methodol*. 1974;36(2):111–147.
21. Schmucker C, Schaeffel F. In vivo biometry in the mouse eye with low coherence interferometry. *Vis Res*. 2004;44(21):2445–2456.
22. Zhou X, Shen M, Xie J, et al. The development of the refractive status and ocular growth in C57BL/6 mice. *Invest Ophthalmol Vis Sci*. 2008;49:5208–5214.
23. Tkatchenko TV, Shen Y, Tkatchenko AV. Analysis of postnatal eye development in the mouse with high-resolution small animal magnetic resonance imaging. *Invest Ophthalmol Vis Sci*. 2010;51(1):21–27.
24. Wisard J, Chrenek MA, Wright C, et al. Non-contact measurement of linear external dimensions of the mouse eye. *J Neurosci Methods*. 2010;187(2):156–166.
25. Chou TH, Kocaoglu OP, Borja D, et al. Postnatal elongation of eye size in DBA/2J mice compared with C57BL/6J mice: in vivo analysis with whole-eye OCT. *Invest Ophthalmol Vis Sci*. 2011;52(6):3604–3612.
26. Wisard J, Faulkner A, Chrenek MA, et al. Exaggerated eye growth in IRBP-deficient mice in early development. *Invest Ophthalmol Vis Sci*. 2011;52(8):5804–5811.
27. Hagan C. When are mice considered old? Available at: https://www.jax.org/news-and-insights/jax-blog/2017/november/when-are-mice-considered-old . Accessed February 11, 2021.
28. Al-Hussaini H, Kam JH, Vugler A, Semo M, Jeffery G. Mature retinal pigment epithelium cells are retained in the cell cycle and proliferate in vivo. *Mol Vis*. 2008;14:1784–1791.
29. Kokkinopoulos I, Shahabi G, Colman A, Jeffery G. Mature peripheral RPE cells have an intrinsic capacity to proliferate; a potential regulatory mechanism for age-related cell loss. *PLoS One*. 2011;6(4):e18921.
30. von Leithner PL, Ciurtin C, Jeffery G. Microscopic mammalian retinal pigment epithelium lesions induce widespread proliferation with differences in magnitude between center and periphery. *Mol Vis*. 2010;16:570–581.
31. Voigt AP, Mulfaul K, Mullin NK, et al. Single-cell transcriptomics of the human retinal pigment epithelium and choroid in health and macular degeneration. *Proc Natl Acad Sci USA*. 2019;116(48):24100–24107.
32. Shibuya M, Okamoto H, Nozawa T, et al. Proteomic and transcriptomic analyses of retinal pigment epithelial cells exposed to REF-1/TFPI-2. *Invest Ophthalmol Vis Sci*. 2007;48(2):516–521.
33. Volland S, Esteve-Rudd J, Hoo J, Yee C, Williams DS. A comparison of some organizational characteristics of the mouse central retina and the human macula. *PLoS One*. 2015;10(4):e0125631.
34. Panda-Jonas S, Jonas JB, Jakobczyk-Zmija M. Retinal pigment epithelial cell count, distribution, and correlations in normal human eyes. *Am J Ophthalmol*. 1996;121(2):181–189.
35. Gomez-Galvez P, Vicente-Munuera P, Tagua A, et al. Scutoids are a geometrical solution to three-dimensional packing of epithelia. *Nat Commun*. 2018;9(1):2960.